SnPb钎料与 Au/Ni/Cu焊盘反应过程中 Au的分布

李福泉[1], 王春青[1], 杜 淼[2], 孔令超[1]
(1.哈尔滨工业大学 现代焊接生产技术国家重点实验室, 哈尔滨 150001; 2.哈尔滨焊接研究所, 哈尔滨 150080)

摘 要: 采用熔融的共晶锡铅钎料熔滴与 Au/Ni/Cu焊盘瞬时接触液固反应形成钎料凸点, 随后进行再流焊及老化。对这一过程中的钎料/焊盘界面金属间化合物组织的演化, 尤其是 Au-Sn化合物的形成及分布进行了研究。结果表明, 钎料熔滴与焊盘液固反应形成了 Au-Sn界面化合物, 铜层未完全反应。在随后的再流焊过程中, 界面处的铜层完全消耗掉, 镍层与钎料反应形成 Ni_3Sn_4 界面组织; 针状的 $AuSn_4$ 化合物分布于钎料基体中。老化条件下分布于钎料基体中的 $AuSn_4$ 重新在界面沉积, 在 Ni_3Sn_4 层上形成 $(Au_xNi_{1-x})Sn_4$ 层。$(Au_xNi_{1-x})Sn_4$ 在界面的沉积遵循分解扩散机制, 并促进富铅相的形成。钎料与焊盘反应过程中 Au-Sn化合物的演化及分布直接影响钎料与焊盘的连接强度。

关键词: 钎料凸点; Au/Ni/Cu; 再流焊; 老化; 金属间化合物
中图分类号: TG111 文献标识码: A 文章编号: 0253-360X(2006)01-53-04

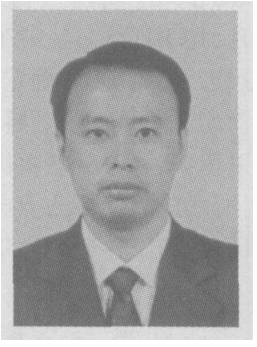

李福泉

0 序 言

球栅阵列(BGA)封装已经逐步成为高密度微电子封装的主流, 其关键技术之一是凸点制作。将一定量熔融的钎料液滴(以下简称熔滴)滴落到金属化焊盘上, 利用熔滴所携带的热量加热焊盘并形成凸点, 是一类新型的凸点制作方法[1~3]。前期工作[4]对共晶 SnPb钎料熔滴与焊盘的接触反应形成凸点过程进行了研究。实际 BGA封装中, 通过钎料凸点实现与基板焊盘的连接; 而钎料凸点还必然要经过组装过程中的再流焊形成焊点, 以实现 BGA封装器件与 PCB电路板之间的连接。同时电子器件老化过程界面化合物的演化对于钎料焊点可靠性有直接的影响。

钎料焊点可靠性与钎料/焊盘界面处的微观组织结构密切相关。钎料与焊盘发生反应, 金属间化合物(IMC)将会在界面处生长, IMC的分布和尺寸对于钎料焊点的强度及其可靠性有重要影响, 了解 IMC的形成机制将会有利于控制其数量、尺寸和分布。

SnPb共晶钎料是电子行业最常见的互连材料。在 BGA封装中, Au/Ni/Cu焊盘得到广泛应用。Au/Ni金属化层是铜焊盘上常用表面层。由于镀镍层有较好的均匀性、耐腐蚀性、与基板的强结合性以及较好的可钎焊性, 因此镀镍涂层成为扩散阻挡层的最佳选择。而 Au因其具有良好的润湿性能和防腐蚀性能而被作为镍表面的保护膜。

作者对 SnPb钎料熔滴在 Au/Ni/Cu焊盘上所形成凸点界面组织进行了研究。对在随后的再流焊及老化条件下钎料与焊盘反应所引起的 Au-Sn化合物演化, 尤其是 Au-Sn化合物在钎料/焊盘界面及钎料基体内的分布进行研究, 并分析了再流焊及老化对钎料与焊盘连接强度的影响。

1 试验材料与方法

将一定质量的钎料熔化, 并达到特定的温度, 从一定的高度滴落到焊盘上的凸点下金属化层(UBM)上, 焊盘被钎料熔滴所携带的热量加热到钎料的熔点温度以上, 钎料熔滴在焊盘上润湿铺展并与焊盘 UBM发生反应, 熔滴凝固后形成凸点。试验材料选用 SnPb共晶钎料, 其中 Sn-37%(质量分数)Pb。所选钎料为一定直径(试验中均为 0.76 mm)的钎料球以保证熔滴的质量。基板材料

收稿日期: 2005-05-10
基金项目: 总装备部预研究项目(51418070105HT0143)

为 BT树脂,焊盘 UBM 的结构自上至下依次为 Au/Ni/Cu. 焊盘直径为 0.6 mm,铜层的厚度为 2 μm,镍层厚度为 7 μm。焊盘外缘有阻焊膜。

凸点成形的两个工艺参数是钎料球的初始温度和下落高度,根据凸点制作要求设定,钎料熔滴初始温度为 400 ℃,下落高度为 1 mm[4]。

对采用钎料熔滴所形成的钎料凸点进行红外再流焊。再流焊工艺参数选择再流峰值温度为 225 ℃,再流时间分别为 30 s、60 s、120 s、180 s. 再流焊后对焊点进行了老化试验,采用 DG/20-002 台式干燥箱,老化温度为 125 ℃,时间为 1 d、4 d、9 d、16 d、25 d. 将所获得的钎料凸点/焊盘进行垂直切片,用 HITACHI-S470场发射扫描电镜分析界面组织形貌,用 EDX 确定生成相化学组成。通常,凸点剪切试验是评价钎料连接可靠性的常用试验方法。采用 KD-0.5型微机控制精密电子机械试验机,对所形成的钎料凸点与焊盘连接进行了剪切强度测试,剪切位移速率为 0.1 mm/min.

2 试验结果与分析

2.1 钎料熔滴/焊盘瞬时接触液固反应界面组织

图 1为 SnPb钎料熔滴初始温度 400 ℃条件下所形成的凸点/焊盘界面微观组织的扫描电镜照片。可以发现,凸点/焊盘界面出现连续层状的金属间化合物,并且有棒状化合物从界面处长出,棒状化合物之间出现白色的富铅相。经 EDX分析,下部靠近镍层的连续层状物的成分为 $AuSn_2$ 和未反应的 Au,上部靠近钎料处棒状化合物成分为 $AuSn_4$。出现金属间化合物层说明,钎料熔滴与焊盘金镀层接触后,Au迅速向液态钎料中溶解并使界面一薄层达到饱和溶解的,从而生成金属间化合物。由于温度较高,Au向熔融钎料中溶解的速度较高,金属间化合物长大明显。但是焊盘在 SnPb钎料熔点(183 ℃)以上温度停留的时间不够长,仍然有一部分 Au未参加反应。生成 $AuSn_4$ 的过程中消耗了大量的 Sn,使局部 Sn的浓度降低从而导致在棒状化合物之间富铅相的形成。

在图 1离界面不远的钎料里发现细小的 $AuSn_4$,即界面金属间化合物脱离界面进入钎料中。这可能与钎料熔滴下落与焊盘撞击过程和凝固过程中,都会产生液态金属的流动,而 Au-Sn化合物较脆,因此在金属流动的作用下导致折断的缘故。同时,冷却过程中较高的冷却速度导致界面处存在较高的应力,也会致使 Au-Sn化合物折断。另一方面,Au在高温下迅速地向熔融钎料中溶解,溶解进入钎料基体中的 Au与 Sn反应在凝固过程中析出 $AuSn_4$。

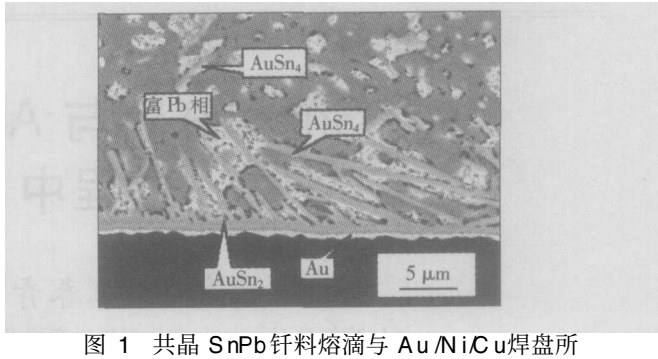

图 1 共晶 SnPb钎料熔滴与 Au/Ni/Cu焊盘所形成的界面微观组织

Fig. 1 Interfacial microstructures between eutectic SnPb solder droplet and Au/Ni/Cu pad

2.2 再流焊条件下界面组织变化

在对 SnPb钎料凸点/焊盘随后进行再流焊的过程中,发现再流焊 30 s后金层完全反应进入钎料中,界面处的化合物层是部分镍层与 Sn反应的产物,经 EDX分析化合物层为 Ni_3Sn_4 层。图 2a所示为 SnPb钎料凸点/焊盘经再流焊 60 s的界面微观组织。可以发现,在 Ni_3Sn_4 层下还存在很厚的镍层

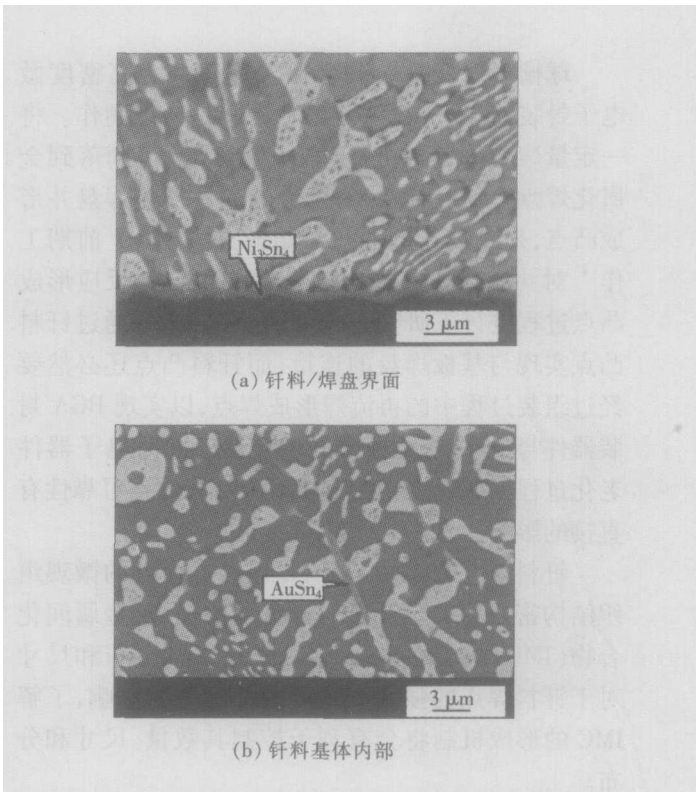

图 2 再流焊 60 s后 SnPb钎料/焊盘界面及距界面 100 μm 的钎料基体内部微观组织

Fig. 2 Interface microstructure between eutectic SnPb solder and pad

未反应，金层在重熔条件下已完全以 Au－Sn化合物的形态进入了钎料基体内部。再流焊后在钎料凸点顶部距界面较远处的钎料基体中仍可以发现 $AuSn_4$ 组织的存在，如图 2b所示为再流焊 60 s后距界面 100 μm的钎料基体内部。可以发现 $AuSn_4$ 以棒状和细小针状形态存在于钎料基体中。再流时间延长，由于液态金属的流动，引起靠近界面钎料基体内的 $AuSn_4$ 组织向远离界面的钎料基体游离。图 3为 再流焊 180 s后远离界面的钎料凸点顶端位置的钎料基体，可以发现针状的 $AuSn_4$ 组织已游离到并分布于钎料凸点的顶端。

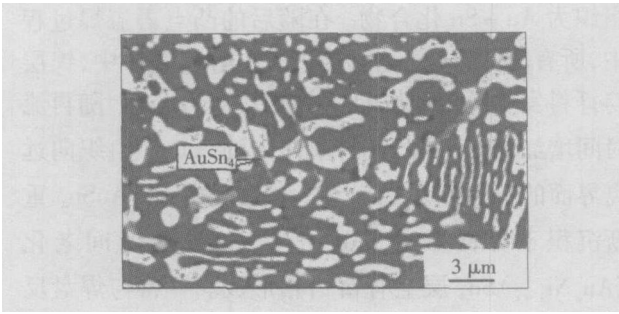

图 3　再流焊 180 s后远离界面的靠近凸点顶端位置钎料基体

Fig. 3　Microstructure of solder bulk at farthest part from interface after 180 s reflow

对再流焊过程中金镀层从界面消失的原因有两种类似的解释，一种为金在熔融 SnPb共晶钎料内部的溶解速度非常快，再流焊期间金镀层完全溶解到熔融钎料内部，在凝固期间与 Sn反应生成 $AuSn_4$ 金属间化合物。另一种解释为钎料再流焊期间在界面处 Sn与 Au反应生成 $AuSn_4$ 金属间化合物，$AuSn_4$ 化合物较脆，在熔融钎料对流作用下进入钎料基体中。然后 $AuSn_4$ 游离到钎料内部。

2.3　老化条件下界面组织变化

图 4所示为钎料凸点 焊盘再流焊 120 s后形成的焊点 125 ℃老化 9 d、25 d的扫描电镜照片。前述研究表明再流焊后未老化的凸点焊盘界面组织为连续的 Ni_3Sn_4 层，$AuSn_4$ 分布在钎料内部。在老化条件下，见图 4可以发现，在 Ni_3Sn_4 层上面出现了一层连续的金属间化合物，EDX 分析表明此化合物层为 $(Au_xNi_{1-x})Sn_4$。$(Au_xNi_{1-x})Sn_4$ 是 $AuSn_4$ 溶解一定数量 Ni形成的，Ni替代并占据部分 Au的晶格。随着老化时间的增加，界面处 $(Au_xNi_{1-x})Sn_4$ 层不断变厚，老化 25 d其厚度达 2.8 μm。$AuSn_4$ 向界面的重新沉积取决于 Ni向 $AuSn_4$ 中溶解降低其吉布斯自由能，界面处的 Ni可对钎料基体内的 $AuSn_4$ 有稳定作用，自由能的降低成为 $AuSn_4$ 向界面沉积形成新相的驱动力，引起 Au的迁移。当 Ni在 $AuSn_4$ 中溶解度达摩尔分数 10%（质量分数 4.87%）时，$AuSn_4$ 相的自由能下降 3 kJ/(g·atoms)[5]。

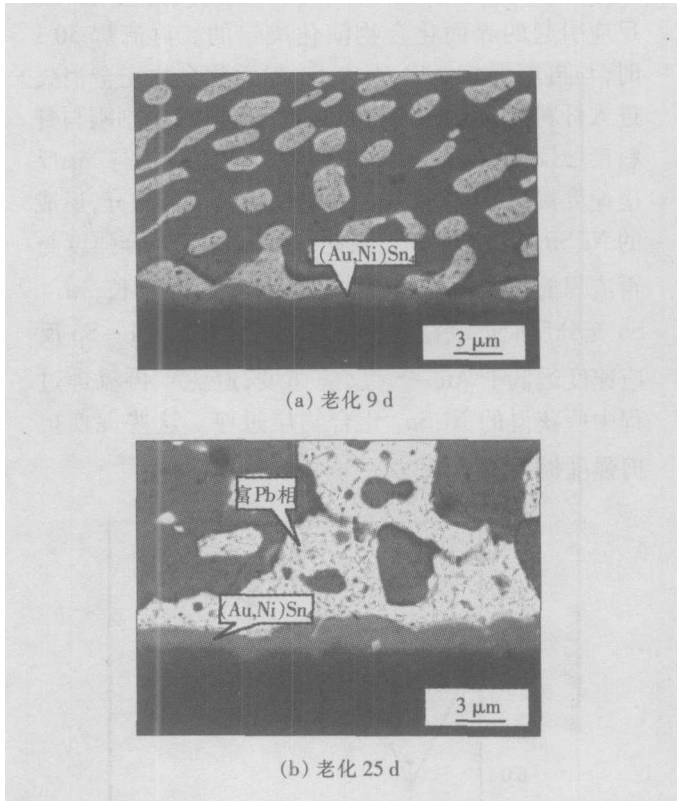

图 4　再流焊 120 s并老化的 SnPb钎料/焊盘界面微观组织

Fig. 4　Interfacial microstructure between eutectic SnPb solder bump and pad after 120 s reflow soldering and aging

可以认为 $(Au_xNi_{1-x})Sn_4$ 在界面的沉积遵循分解扩散机制，即 $AuSn_4$ 并不能以整体的形式返回界面，而是在返回界面之前发生了分解，即

$$AuSn_4 = Au + 4Sn$$

分解出来的 Au原子扩散回界面处与 Ni_3Sn_4 反应

$$xAu + \frac{4}{3}(2+x)Sn + \frac{(1-x)}{3}Ni_3Sn_4 = (Au_xNi_{1-x})Sn_4$$

由于方程中每个 Au原子，将需要 7.26个 Sn原子参与反应，生成 $(Au_xNi_{1-x})Sn_4$ 将消耗大量的 Sn原子。导致在老化后 $(Au_xNi_{1-x})Sn_4$ 层上有富铅相形成。如图 4所示，老化时间短的情况下，靠近界面 $(Au_xNi_{1-x})Sn_4$ 层出现了块状富铅相。随着老化时间增加，更多的 $AuSn_4$ 向界面重新沉积，消耗大量的 Sn，块状富铅相变大。老化时间达 25 d情况下，在 $(Au_xNi_{1-x})Sn_4$ 层上方发现有连续的一层富铅相。

2.4 再流焊及老化对凸点剪切载荷的影响

对不同再流时间下最大剪切载荷测试结果如图 5所示，由图可以发现再流焊后最大剪切载荷变化情况。与再流焊前获得的凸点最大剪切载荷相比，再流焊 30 s时凸点最大剪切载荷下降，随后最大剪切载荷升高。这是由不同再流时间钎料与焊盘反应引起的界面化合物演化决定的。再流焊 30 s时，与再流焊前相比，Au-Sn界面化合物完全消失进入钎料内，金化合物层完全消耗掉，镍层刚刚与钎料接触反应。而 Ni与 Sn的反应比较 Au与 Sn反应速度慢得多，钎料与焊盘镍层反应很不充分，形成的 Ni_3Sn_4化合物过薄，因此钎料与焊盘结合强度与再流焊前相比明显下降。随着再流时间延长，Ni-Sn充分反应形成稳定的 Ni_3Sn_4化合物。Ni-Sn反应速度远低于 Au-Sn反应速度，避免了再流焊过程中所获得的 Ni_3Sn_4化合物层过厚。这些促使抗剪强度提高。

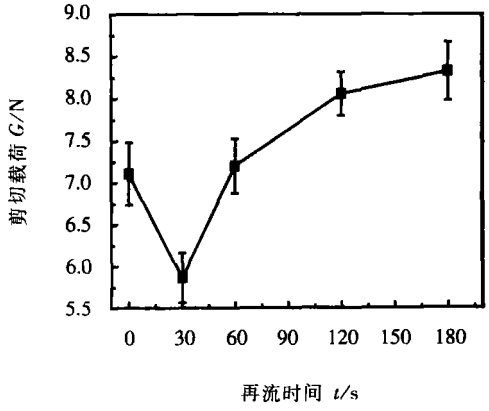

图 5 再流焊对 SnPb凸点剪切载荷的影响

Fig. 5 Influence of reflow time on shear load of SnPb eutectic solder bump

图 6所示为老化对 SnPb钎料凸点剪切载荷的影响。由于老化促使再流焊过程中已进入钎料内部的 $AuSn_4$重新沉积于界面，形成脆性的 $(Au_xNi_{1-x})Sn_4$，同时出现富铅相，必然引起凸点最大剪切载荷降低。随着老化时间增加，$(Au_xNi_{1-x})Sn_4$层增厚，并且富铅相逐渐成为层状，剪切过程中 $(Au_xNi_{1-x})Sn_4$层与富铅层间易于发生断裂，凸点最大剪切载荷进一步降低。

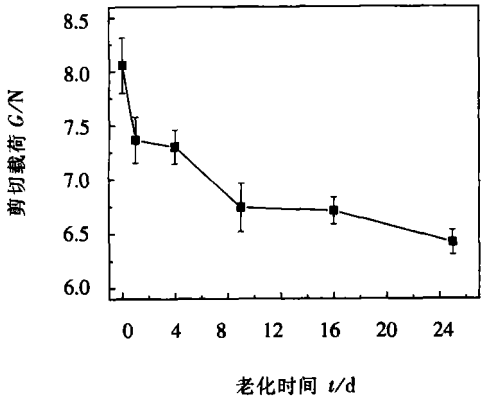

图 6 老化对 SnPb凸点剪切载荷的影响

Fig. 6 Influence of aging at 125 ℃ on shear load of SnPb eutectic solder bump

3 结 论

SnPb钎料熔滴 Au/Ni/Cu焊盘所形成的界面组织为 Au-Sn化合物。在随后的凸点再流焊过程中，所有的 Au-Sn化合物进入了钎料基体中，镍层与钎料发生反应形成的界面组织为 Ni_3Sn_4。随再流时间增加，靠近界面钎料基体内的 $AuSn_4$组织向远离界面的钎料基体内游离。老化过程中，$AuSn_4$重新沉积于界面形成 $(Au_xNi_{1-x})Sn_4$。长时间老化 $(Au_xNi_{1-x})Sn_4$层上有富铅相形成。钎料与焊盘反应过程中 Au-Sn化合物的演化及分布直接影响钎料与焊盘的连接强度。

参考文献：

[1] Liu Q B, Orme M. High precision solder droplet printing technology and the state of theart[J]. Journal of Materials Processing Technology, 2001, 115: 271-283.

[2] Hayes D J, Cox W R, Grove M E. Micro-jet printing of polymers and solder for electronics manufacturing[J]. Journal of Electronics Manufacturing, 1998, 8(3-4): 209-216.

[3] Motulla G, Kasulke P, Heinricht K, *et al*. A low cost bumping process for flip chip technology using electroless nickel and solder ball placement[A]. 1997 IEMT/IMC symposium[C]. Tokyo: the Organizing Committee, 1997. 174-181.

[4] 李福泉，王春青，田德文，等. SnPb钎料熔滴与 Au/Ni/Cu焊盘的反应过程[J]. 中国有色金属学报，2004, 14(7): 1139-1143.

[5] Zeng K, Tu K N. Six cases of reliability study of Pb-free solder joints in electronic packaging technology[J]. Materials Science and Engineering, 2002, R38: 55-105.

作者简介：李福泉，男，1972年出生，博士研究生。主要从事电子封装与组装、微连接及钎焊等研究工作，发表论文 10篇。

Email: lifuquan@hit.edu.cn

welded surface microstructure of steel before welding. If only one surface is eligible for ultra-fining, the tensile strength of the joint will be also up to that of 40Cr base metal, but the welding time is slightly longer. ISSW belongs to the little deformation welding, the deformation of joint is mainly located in the quenched area near original interface. The deformation of T10A side is larger than that of 40Cr side.

Key words: steel; microstructure; ultra-fining treatment; superplastic solid-state welding; process

Phase transformation diffusion bonding technology for titanium alloy to stainless steel QIN Bin[1], SHENG Guang-min[1,2], HUANG Jia-wei[1], LI Cong[2] (1. College of Material Science and Engineering, Chongqing University, Chongqing 400044, China; 2. National Key Laboratory for Nuclear Fuel and Material, Nuclear Power Institute of China, Chengdu 610041, China). p41 - 44, 48

Abstract: The joints of titanium alloy (TA17) and stainless steel (0Cr18Ni9Ti) were obtained by phase transformation diffusion bonding. Effect of parameters on strength of the joint was investigated, and the optimum parameters for bonding are as follows: maximum cyclic temperature is 890 ℃, minimum cyclic temperature is 800 ℃, number of cyclic times is 10, bonding pressure is 5 MPa and heating velocity is 30 ℃/s. Strength of the joint under the optimum condition is 307 MPa, and the time for bonding is 160 s. Scanning electron microscopy (SEM), energy dispersive spectroscopy (EDS) and X-ray diffraction (XRD) were used to study the fracture appearance of the joint. The study showed that the fracture takes place at somewhere between FeTi and β-Ti layers, and the FeTi layer is the weakest point in the joints. The joint was analyzed by EDS and the ternary phase diagram for Fe-Cr-Ti. The results indicated the presence of σ, Fe_2Ti, FeTi and β-Ti in the reaction zone between stainless steel and titanium alloy.

Key words: titanium alloy; stainless steel; phase transformation; diffusion bonding

Metal transfer of twin-wire indirect arc argon welding CAO Mei-qing, ZOU Zeng-da, DU Bao-shuai, QU Shi-yao, WANG Xin-hong, LI De-gang (School of Material Science and Engineering, Shandong University, Jinan 250061, China). p45 - 48

Abstract: The metal transfer and the corresponding arc voltage and welding current in twin-wire indirect arc argon welding was investigated with high speed camera system based on a xenon lamp source and digital oscillograph. Results showed that with the different matching of welding current and arc voltage, the mode of metal transfer consists of short circuiting transfer, globular transfer, mixing transfer, projected transfer and streaming transfer etc. With the increasing of welding current, the droplet size reduces, and the droplet is refined. With the raising of arc voltage, the size of droplet reduces. There is well corresponding relationship between metal transfer mode and the oscillogram of volgtage and welding.

Key words: indirect arc; metal transfer; short circuiting transfer; streaming transfer

Autonomous seam tracking based on local vision in arc robotic welding ZHOU Lü, CHEN Shan-ben, LIN Tao, CHEN Wen-jie (Welding Institute, Shanghai Jiaotong University, Shanghai 200030, China). p49 - 52

Abstract: A method of autonomous seam tracking in arc robotic welding was presented. It could make the robot get rid of traditional teaching and playing back mode and automatically acquired the special coordinates of welding seam. The master computer continuously processed local area images in front of the torch in the images which were acquired by a CCD camera to measure the deviation between the torch and the seam and the orientation of the seam. At the same time, the computer controlled the robot to make the torch move forward along the seam and recorded the seam's coordinates in the robotic basic reference frame which were corrected by the deviations. After the torch arrives at the end-point of the seam, the computer controlled the robot to move the torch to the first record coordinate and begin to weld. Experiments were made on the curves seam workpieces of mild steel and aluminum alloy workpieces. The result showed that this method has good practicability.

Key words: image processing; arc welding robot; autonomous seam tracking; local vision

Distribution of Au during reaction of eutectic SnPb solder and Au/Ni/Cu pad LI Fu-quan[1], WANG Chun-qing[1], DU Miao[2] (1. National Key Laboratory of Advanced Welding Production Technology, Harbin 150001, China; 2. Harbin Welding Institute, Harbin 150080, China). p53 - 56

Abstract: Solder bump was fabricated with Sn-Pb eutectic solder droplet on Au/Ni/Cu pad. The solder/pad was then subject to reflow soldering and aging at 125 ℃. The IMC evolution at solder/pad interface during this process, especially the formation and distribution of Au-Sn compound were investigated. The results showed that Au-Sn compound forms at solder/pad interface during contact reaction, and Au does not react fully with solder droplet. During the subsequent reflow soldering, all Au layer at interface is consumed. Ni layer reacts with solder, which leads to the formation of Ni_3Sn_4 compound at the interface. Acicular $AuSn_4$ can be found in the solder bulk. $AuSn_4$ particles redesposites at the interface as a continuously $(Au_xNi_{1-x})Sn_4$ layer during aging at 125 ℃. The redesposited $(Au_xNi_{1-x})Sn_4$ at solder/pad interface follows decomposition-diffusion mechanism. At the same time, a lead-rich phase emerges with $AuSn_4$ redeposition at the interface. The shear strength of soldered joint is mainly determined by this evolution and distribution of Au-Sn compound.

Key words: solder bump; Au/Ni/Cu; reflow; ageing; interme

tallic compound

Experimental study on operative performance of high cellulose covered electrode for pipe welding LIU Hai-yun[1,2], LI Zhuo-xin[1], SHI Yao-wu[1] (1. School of Material Science and Engineering, Beijing University of Technology, Beijing 100022, China; 2. College of Material Science and Engineering, Taiyuan University of Science and Technology, Taiyuan 030024, China). p57 - 60

Abstract: Based on SiO_2-TiO_2-MgO-FeO slag system, a great deal of operative performance experiments for high cellulose covered electrode were carried out. The feature of metal transfer of the electrode was revealed. The results showed that operative performance in the vertical down welding can be improved through fine droplet, increasing chemical reactive heat in arc area, raising arc blow force. Using sodium water glass with super low mode, carbonization and press coating problems during manufacture can be solved.

Keywords: high cellulose covered electrode; operative performance; pipe welding

Improving corrosion resistance of low carbon steel welded joint by magnetic treatment LIN Jian-a, ZHAO Hai-yan, CAI Zhi-peng, LIU An-li, WU An-na, YAN Dong-yang (Department of Mechanical Engineering, Tsinghua University, Beijing 100084, China). p61 - 64, 68

Abstract: The effect of magnetic treatment on corrosion resistance of low carbon steel joint was studied. The experiment showed that the etching rating can be reduced by magnetic treatment at a relative level of 2.58%. A finite element analysis was carried out for predicting the residual stress that influenced the corrosion resistance of joint. In addition, a significance test for the change of the etching rating after magnetic treatment was performed. It showed that the change of the etching rating after treatment is out of the range of experimental error with the significance coefficient of 5%. It could be concluded that the corrosion resistance of low carbon steel joint can be improved by magnetic treatment with a significance level of 5%.

Keywords: magnetic treatment; etching rating; weld residual stress; numerical simulation; significance test

Friction stir welding of 2219-O aluminum alloy CHEN Ying-chun, LIU Hui-jie, FENG Ji-cai (State Key Laboratory of Advanced Welding Production Technology, Harbin Institute of Technology, Harbin 150001, China). p65 - 68

Abstract: 2219-O aluminum alloy was friction stir welded to investigate the effect of friction stir welding on its microstructure and mechanical properties in this paper. The microstructures of different zones in the joint were analyzed by optical microscopy, and the mechanical properties of the joint were evaluated by means of tensile tests. Microstructural analyses indicated that the weld nugget zone (WNZ) is composed of fine isometric grains because of continuously dynamic recrystallization, and more precipitates formed in this zone. In the thermal-mechanical affected zone (TMAZ), the grains have experienced incomplete recrystallization due to seriously plastic deformation, and some small grains begin to nucleate. In the heat affected zone (HAZ), all the grains are coarsened. Tensile tests showed that the tensile strength of the joint is the same as that of the base metal, and the fracture occurs in the base metal when the tool rotation speed was 800 rpm and the welding speed was less than 400 mm/min. On the other hand, when the welding speed was greater than 400 mm/min, the mechanical properties of the joint significantly degrade and the joint fractures at the defect location because of the formation of a defect in the WNZ.

Keywords: friction stir welding; aluminum alloy; microstructural characteristics; mechanical properties

Self-shielded metal cored wire for hardfacing with high hardness and abrasion resistance JIANG Min, LI Zhuo-xin, JIANG Jian-min, SHI Yao-wu (School of Material and Engineering, Beijing University of Technology, Beijing 100022, China). p69 - 71

Abstract: The high-chromium cast iron type self-shielded metal cored wire (SSMCW) for hardfacing with good operative performance and appearance was developed. The hardness of deposited metal exceeds HRC60, and the wearing resistance is 21 times higher than that of Q235 steel. The mechanism of self-shielding was researched. When manganese content arrives at 5wt% in wire, porosity can be avoided, while Ti+Fe content exceeds 10wt%, pits will appear in the weld of SSMCW. The microstructure of deposited metal consists of martensite and a little residual austenite, and the abrasive resistant hard phase M_7C_3 distributes uniformly in martensite matrix.

Keywords: high hardness; high abrasion resistance; self-shielded metal cored wire for hardfacing

Correlation of acoustic signals and weld depth in laser welding LIU Jing-lei[1,2], CHEN Yan-bin[2], XU Qing-hong[2] (1. School of Mechanical and Power Engineering, East China University of Science and Technology, Shanghai 200237, China; 2. School of Material Science and Engineering, Harbin Institute of Technology, Harbin 150001, China). p72 - 75, 80

Abstract: Laser welding is accompanied with a strong acoustic signal which contains a considerable amount of information on the welding process and indicates certain aspects of weld quality. The characteristics of weld acoustic signal during laser cladding were analyzed in details. The intensity and power spectrum components of acoustic signals were found to be a match for the weld depth. The dominant power spectra covered by the experimental set-up ranged from 2 to 10 kHz, where several obvious spectrum lines were detected. The amplitude of acoustic signals decreases and the acoustic power spectrum lines change from intensive and simple to